Published in "Bioconjugate Chemistry 20(7): 1349–1355, 2009"
which should be cited to refer to this work.

Photoinitiated Coupling of Unmodified Monosaccharides to Iron Oxide Nanoparticles for Sensing Proteins and Bacteria

Li-Hong Liu,[†] Hervé Dietsch,[‡] Peter Schurtenberger,[‡] and Mingdi Yan*,[†]

Department of Chemistry, Portland State University, P.O. Box 751, Portland, Oregon 97207-0751, and Adolphe Merkle Institute and Fribourg Center for Nanomaterials, University of Fribourg, Route de l'ancienne Papeterie CP 209, CH-1723 Marly 1, Switzerland.

We report a versatile approach for the immobilization of unmodified monosaccharides onto iron oxide nanoparticles. Covalent coupling of the carbohydrate onto iron oxide nanoparticle surfaces was accomplished by the CH insertion reaction of photochemically activated phosphate-functionalized perfluorophenylazides (PFPAs), and the resulting glyconanoparticles were characterized by IR, TGA, and TEM. The surface-bound D-mannose showed the recognition ability toward *Concanavalin A* and *Escherichia coli* strain ORN178 that possesses mannose-specific receptor sites. Owing to the simplicity and versatility of the technique, together with the magnetic property of iron oxide nanoparticles, the methodology developed in this study serves as a general approach for the preparation of magnetic glyconanoparticles to be used in clinical diagnosis, sensing, and decontamination.

INTRODUCTION

Naturally occurring carbohydrates and glycoconjugates (glycoproteins, glycolipids) present at the surface of nearly every cell in the living system are known to play crucial roles in biological events as recognition sites between cells and factors. They can trigger various phenomena such as cell growth, inflammatory responses, or viral infections. Surface-exposed carbohydrate moieties that are characteristic of a given microbe may serve as key biomarkers for pathogen and toxin identification, diagnosis, and vaccine development. Carbohydrates as a detection platform have recently emerged and have demonstrated tremendous potential to achieve superior sensitivity and selectivity (*1*−*4*). Compared to antibodies used in immunoassays that are often fragile and unstable, carbohydrates are stable entities. Carbohydrate-based assays have the potential to be an alternative benchmark detection technology for a wide range of biomolecules including proteins, bacteria, pathogens, and toxins (*5*).

A key technology requirement in receptor/ligand-based sensing and detection is the surface conjugation chemistry leading to efficient and effective coupling of ligands to solid substrates (*6*). The performance of the device, the detection sensitivity, and the dynamic range are largely governed by the ligand to be immobilized, the nature of the coupling chemistry, the ligand density, and the presentation. There is a great demand for effective conjugation chemistry that is general, versatile, and can accommodate ligand diversity and give stable interfaces, yet is simple and reproducible. Reported strategies for the covalent immobilization of carbohydrates on surfaces mostly rely on conventional coupling chemistry, such as amines with ester (*7, 8*) thiols with maleimides (*9, 10*), and azide with alkynes (*11, 12*), which requires sometimes laborious synthesis of carbohydrates having a specific functional group or tether. Coupling chemistry that does not require chemical derivatization of carbohydrates is appealing. There are a few methods reported in literature. One approach uses hydrazide-modified gold substrates, where the hydrazide reacts with the terminal aldehyde group of the carbohydrates (*13, 14*). A similar approach employs amine-functionalized surfaces, and the coupling with carbohydrates takes place by reductive amination to yield an amine conjugate (*15, 16*). In both cases, reducing sugars are necessary, and for monosaccharides, the coupled products often become acyclic and lose their binding affinity. Photochemically initiated immobilization and patterning of biological molecules has been explored (*17*), although few reports have focused on carbohydrates (*18, 19*).

We have developed a photochemically initiated coupling chemistry that employs functionalized perfluorophenyl azides (PFPAs) to attach molecules and materials to solid substrate surfaces (*20*−*22*). Upon light activation, the azide moiety converts to a highly reactive nitrene that, notably, inserts into CH and NH bonds, creating highly robust covalent linkages. We have successfully employed PFPAs in surface modification, targeting polymeric materials that lack reactive functional groups for surface coupling (*23, 24*). Carbohydrates, being complex in structure and challenging to chemically derivatize, are another class of compounds that are well-suited for the PFPA photocoupling chemistry. The design of our approach is to prepare PFPA-functionalized iron oxide nanoparticles that can be subsequently used to covalently couple, in principle, any carbohydrate structures by way of the insertion reactions of photochemically activated nitrene species.

Iron oxide nanoparticles are attractive due to their inherent magnetic properties that make them useful for magnetic resonance imaging, magnetic field-assisted transport, as well as sensing and separation (*25*−*27*). In addition, iron oxide nanoparticles are nonporous, which avoid delay due to diffusion, and thus the equilibrium is reached rapidly and fast response can be achieved. A number of methods have been reported for functionalizing iron oxide nanoparticles with organic compounds (*28, 29*) such as silanes (*30, 31*) and phosphoric acids (*32*−*38*). Silanes form robust siloxane bonds with surface −OH groups; the drawback is the self-condensation reaction leading to multilayer formation or deposition of aggregates on the substrate surface. Phosphates, on the other hand, do not undergo self-condensation reactions. These agents couple with surface −OH groups creating the stable Fe−O−P structure (*28, 32*).

* To whom correspondence should be addressed. Phone: 503-725-5756, E-mail: yanm@pdx.edu.
[†] Portland State University.
[‡] University of Fribourg.

Here, we report the synthesis of phosphate-functionalized PFPAs and their uses for the covalent immobilization of monosaccharides on iron oxide nanoparticles. The recognition ability of the surface-bound ligands are tested using *Concanavalin A* (*Con A*), an oligomannose-binding lectin, and *Escherichia coli* (*E. coli*) strain ORN178 that possesses mannose-specific receptor sites (*39*). *Con A* and *E. coli* also serve as the model systems allowing us to test the ability of these carbohydrate-functionalized iron oxide nanoparticles for sensing and detecting proteins and bacteria.

EXPERIMENTAL SECTION

Materials and Instrumentation. Chemicals and solvents were purchased from TCI, Sigma-Aldrich, ACROS, or Fisher Scientific. Methylene chloride was distilled from calcium hydride. Triethylamine was distilled before use. All other solvents and commercial grade reagents were used without further purification. Milli-Q water having a resistivity of 18.2 $mW \cdot cm^{-1}$ was used for the synthesis of spindle-type hematite particles. ^1H NMR and ^{13}C NMR spectra were recorded in $CDCl_3$ on a Bruker AMX-400 MHz spectrometer. Chemical shifts were reported in parts per million (ppm) relative to TMS and referenced to the residual solvent. Elemental analysis was performed by Quantitative Technologies Inc. (Whitehouse, NJ). Infrared spectra were obtained on a Perkin-Elmer 2000 series FT-IR spectrometer. TEM images were obtained on a JEOL 100C transmission electron microscope. Photolysis was carried out at the ambient temperature with a 450 W medium pressure Hg lamp (Hanovia). The lamp reached its full power after a 2 min warmup to an intensity of 5.0 mW/cm^2, as measured by a model UVX radiometer and UVX-36 sensor (Upland, CA). A 280 nm optical filter was used during irradiation. Thermogravimetric analysis (TGA) was performed on a Perkin-Elmer TGA7 Analyzer. Samples were combusted in nitrogen flow at a heating rate of 10 °C/min from 50 to 900 °C.

2-(2′-(2″-(4-Azidoethoxy)ethoxy)ethanol (3). 2-(2′-(2″-Chloroethoxy)ethoxy)ethanol (0.5 g, 2.97 mmol), NaI (0.09 g, 0.6 mmol), and NaN_3 (2.0 g, 30 mmol) were dissolved in water (10 mL), and the solution was stirred at 50 °C for 48 h. The reaction mixture was then filtered, and the aqueous phase was extracted with ethyl acetate (4 × 10 mL). The organic extracts were collected and evaporated to give **3** as a light yellow liquid (0.4 g, 77%). ^1H NMR (400 MHz, $CDCl_3$, δ): 3.72 (t, 2H, J = 5.0 Hz), 3.68 (m, 6H), 3.60 (t, 2H, J = 5.0 Hz), 3.40 (t, 2H, J = 5.0 Hz), 3.19 (br, 1H). ^{13}C NMR (100 MHz, $CDCl_3$, δ): 72.63, 70.59, 70.34, 69.98, 61.56, 50.61.

2-(2′-(2″-Aminoethoxy)ethoxy)ethanol (4). 2-(2′-(2″-(4-Azidoethoxy)ethoxy)ethanol (**3**) (400 mg, 2.4 mmol) was dissolved in dry THF (10 mL), and the solution was cooled to 0 °C. Triphenyl phosphine (600 mg, 2.4 mmol) was added, and the reaction mixture was stirred at room temperature for 10 h. Water (0.12 mL, 6.7 mmol) was added, and the mixture was stirred for another 5 h. The reaction mixture was diluted with water and washed with toluene (3 × 10 mL). The aqueous layers were collected and evaporated to give **4** as a colorless liquid (240 mg, 70% crude). This compound was used directly in the next step without further purification.

4-Azido-2,3,5,6-tetrafluoro-*N*-(2-(2′-(2″-hydroxyethoxy)-ethoxy)ethyl)benzamide (5). Dry CH_2Cl_2 (10 mL) was added to a mixture of *N*-succinimidyl 4-azidotetrafluorobenzoate (*40*) (400 mg, 1.2 mmol) and 2-(2′-(2″-aminoethoxy)ethoxy)ethanol (**4**) (180 mg, 1.2 mmol) via syringe, and the mixture was purged with argon for 30 min and stirred at room temperature for 6 h. Water (10 mL) was added, and the mixture was extracted by $CHCl_3$ (3 × 10 mL). The organic layers were combined, dried over anhydrous Na_2SO_4, and evaporated in vacuo. The residual was purified by column chromatography (10/4/0.5, ethylacetate/hexanes/methanol) to give **5** as a white waxy solid (180 mg, 41%).^1H NMR (400 MHz, $CDCl_3$, δ): 7.04 (1H), 3.65 (m, 10H), 3.55 (t, 2H, J = 5.0 Hz), 2.69 (br, 1H). ^{13}C NMR (100 MHz, $CDCl_3$, δ): 157.93, 145.28, 142.78, 141.74, 139.08, 121.60, 111.85, 72.47, 70.28, 70.23, 69.47, 61.51, 39.99. Anal. Calcd. for $C_{13}H_{14}F_4N_4O_4$: C 42.63; H 3.85; N 15.30. Found: C 42.43; H 3.87; N 15.27.

2-(2′-(2″-(4-Azido-2,3,5,6-tetrafluorobenzamido)ethoxy)-ethoxy)ethyl Dihydrogen Phosphate (1). 4-Azido-2,3,5,6-tetrafluoro-*N*-(2-(2′-(2″-hydroxyethoxy)ethoxy)ethyl) benzamide (**5**) (180 mg, 0.49 mol) was dissolved in dry CH_2Cl_2, and the solution was purged with argon. Anhydrous triethylamine (0.1 mL, 0.7 mmol) was added, and the mixture was cooled to 0 °C with an ice bath before $POCl_3$ (0.06 mL, 0.7 mmol) was added dropwise. The reaction mixture was allowed to warm to room temperature and stirred for another 6 h. Water (10 mL) was added, and the mixture was stirred for 1 h. The reaction mixture was extracted with $CHCl_3$ (3 × 10 mL). The organic layers were collected, dried over anhydrous Na_2SO_4, and evaporated to give **1** as a light yellow, highly viscous clear liquid (120 mg, 55%). ^1H NMR (400 MHz, $CDCl_3$, δ): 6.94 (br, 1H), 4.44 (m, 2H), 3.80 (m, 2H), 3.67 (m, 8H). ^{13}C NMR (100 MHz, $CDCl_3$, δ): 157.94, 145.30, 142.80, 141.76, 139.09, 121.63, 111.82, 71.03, 70.77, 70.32, 69.43, 68.97, 40.01. Anal. Calcd. for $C_{13}H_{15}F_4N_4O_7P$: C 34.99; H 3.39; N 12.56. Found: C 34.72; H 3.18; N 12.23.

4-Azido-2,3,5,6-tetrafluoro-*N*-(8-hydroxyoctyl)benzamide (6). *N*-Succinimidyl 4-azidotetrafluoro benzoate (200 mg, 0.6 mmol) and 8-aminooctan-1-ol (90 mg, 0.6 mmol) were added to dry CH_2Cl_2 (10 mL), and the solution was purged with argon for 30 min and stirred at room temperature for 6 h. Water (10 mL) was then added, and the mixture was extracted with $CHCl_3$ (3 × 10 mL). The organic layers were combined, dried over anhydrous Na_2SO_4, and evaporated in vacuo. The residual was purified by column chromatography (10/4/0.5, ethylacetate/hexanes/methanol) to give **6** as a white power (110 mg, 50%). ^1H NMR (400 MHz, $CDCl_3$, δ): 5.96 (s, 1H), 3.64 (t, 2H, J = 7.0 Hz), 3.45 (q, 2H, J = 7.0 Hz), 1.59 (m, 4H), 1.35 (m, 8H). ^{13}C NMR (100 MHz, $CDCl_3$, δ): 157.59, 145.34, 142.79, 141.63, 139.15, 121.82, 111.61, 62.99, 40.33, 32.70, 29.27, 29.23, 29.10, 26.65, 25.61. Anal. Calcd. for $C_{15}H_{18}F_4N_4O_2$: C 49.72; H 5.01; N 15.46. Found: C 49.63; H 5.18; N 15.47.

8-(4-Azido-2,3,5,6-tetrafluorobenzamido)octyl Dihydrogen Phosphate (2). 4-Azido-2,3,5,6- tetrafluoro-*N*-(8-hydroxyoctyl)benzamide (**6**) (250 mg, 0.69 mmol) was dissolved in dry THF (10 mL), and the solution was purged with argon. Anhydrous triethylamine (0.13 mL, 0.9 mmol) was added, and the mixture was cooled to 0 °C with an ice bath before $POCl_3$ (0.08 mL, 0.9 mmol) was added dropwise. The reaction mixture was allowed to warm to room temperature and stirred for another 6 h. Water (10 mL) was added, and the mixture was stirred for another 1 h. The reaction mixture was extracted with $CHCl_3$ (3 × 10 mL). The organic layers were collected, dried over anhydrous Na_2SO_4, and was evaporated to give **2** as a light amber viscous liquid (140 mg, 45%). ^1H NMR (400 MHz, $CDCl_3$, δ): 7.01 (s, 1H), 4.33 (m, 2H), 3.39 (q, 2H, J = 7.0 Hz), 1.81 (m, 2H), 1.59 (t, 2H, J = 7.0 Hz), 1.36 (m, 8H). ^{13}C NMR (100 MHz, $CDCl_3$, δ): 158.05, 145.13, 142.63, 141.69, 139.04, 121.61, 111.73, 72.57, 40.31, 29.42, 29.04, 28.91, 28.76, 26.54, 25.11.

Preparation of Spindle-Type Hematite α-Fe_2O_3. The nanoparticles were synthesized following a slightly modified literature procedure (*41*). In a typical reaction, $Fe(ClO_4)_3 \cdot 6H_2O$ (11.56 g), NaH_2PO_4 (162 mg), and urea (1.50 g) are solubilized into 250 mL of Milli-Q water at room temperature. The obtained solution was sonicated for 2 h, transferred to a preheated oven at 100 °C for 24 h, and then cooled down to room temperature.

Scheme 1. Functionalization of Hematite Nanoparticles with 1 Followed by Coupling of D-Mannose and Subsequent Binding with *Con A*

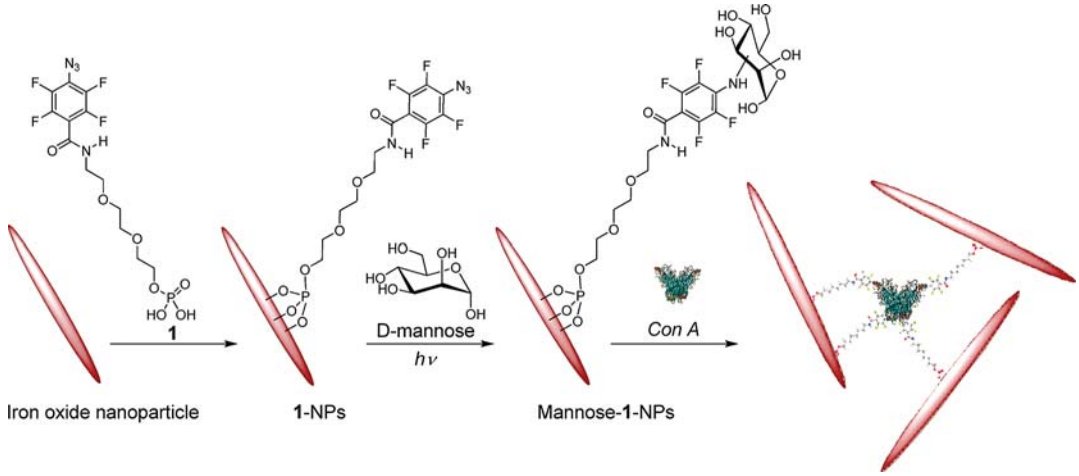

After settling, half of the supernatant was removed and the rest of the mixture was centrifuged. The solid was cleaned 5 times at 10 000 rpm for 20 min each with Milli-Q water. The obtained brick red hematite nanoparticles were stored in Milli-Q water.

Preparation of Magnetite Fe_3O_4 Nanoparticles. Magnetite Fe_3O_4 nanoparticles were prepared by the coprecipitation method (*4, 42*). The Fe^{3+} solution (1 M) was prepared by dissolving ferric chloride hexahydrate ($FeCl_3 \cdot 6H_2O$) in 2 M HCl, and the Fe^{2+} solution (1 M) was prepared by dissolving ferrous sulfate heptahydrate ($FeSO_4 \cdot 7H_2O$) in 2 M HCl. The two solutions, 100 mL of Fe^{3+} and 50 mL of Fe^{2+}, were mixed in a degassed flask. NH_4OH (30%) was added dropwise until the solution pH reached 11. The mixture was stirred vigorously for 30 min at room temperature. The resulting black precipitates were isolated by applying a permanent external magnet and washed 3 times with Milli-Q water. The mixture was then centrifuged, and the solid washed copiously with ethanol to give magnetite Fe_3O_4 nanoparticles.

Preparation of PFPA-Functionalized Iron Oxide Nanoparticles. Hematite (α-Fe_2O_3) and supraparamagnetic (Fe_3O_4) nanoparticles were functionalized with PFPA using the following procedure (*33*). PFPA **1** or **2** and nanoparticles (1:1 w/w, 50 mg each) were mixed in $CHCl_3$ (15 mL), and the mixture was sonicated for 30 min until the particles were well-dispersed. Excess **1** or **2** was removed by copiously washing the nanoparticles with ethanol and centrifuging. Functionalized hematite nanoparticles were labeled as **1**-NP and **2**-NP, respectively, and functionalized Fe_3O_4 nanoparticles were labeled as **1**-Fe_3O_4-NPs.

Coupling Carbohydrates to PFPA-Functionalized Nanoparticles. PFPA-functionalized nanoparticles (5 mg) and the carbohydrate solution (50 μL, 1 mg/mL) were added to water/ethanol (1.5 mL), and UV irradiated for 30 min with a medium pressure Hg lamp with a 280 nm long-path optical filter. The irradiation time of 30 min was determined by FTIR when the azide antisymmetric stretch at 2126 cm^{-1} completely disappeared. The resulting nanoparticles were washed 5 times with water and 3 times with ethanol, and stored in ethanol for further uses.

Binding of Con A to Carbohydrate-Functionalized Nanoparticles. Mannose-functionalized hematite nanoparticles (mannose-**1**-NPs) was incubated with a solution of pH 7.4 PBS buffer containing 0.1% Tween 20 and 3% BSA (w/v) for 30 min and washed with pH 7.4 PBS buffer containing 0.1% Tween 20 for 20 min. The nanoparticles (500 μg/mL) were then incubated with a solution of *Con A* (15 mg/mL) in pH 7.4 PBS containing 0.01% Tween 20 for 6 h at room temperature. The resulting nanopartilces were washed thoroughly with the buffer solution followed by five times with Milli-Q water.

Binding of Mannose-1-NPs to *E. coli* K-12 Strains ORN178 and ORN208. *E. coli* ORN178 and ORN208 were grown in the Luria-Bertain Broth medium at 37 °C to an optical density of 0.9 at 600 nm (approximately 10^9 cells per mL) and precipitated by centrifugation at 3000 rpm for 4 min (*43*). After centrifuging-suspending twice with pH 7.4 PBS buffer, the bacteria (500 μL) was mixed with 500 μL mannose-functionalized nanoparticles (500 μg/mL), and the mixture was gently shaken at room temperature for 1 h.

Transmission Electron Microscopy (TEM). Samples of *E. coli* ORN178 and ORN208 treated with mannose-**1**-NPs were placed onto a 200 mesh carbon-coated copper grids, and the suspension was allowed to settle for 1 min, and the excess liquid was removed by a filter paper. A drop of 1% phosphotungstic acid was used to negatively stain the samples for 1 min before they were examined by TEM.

RESULTS AND DISCUSSION

The design of our approach is to prepare PFPA-functionalized iron oxide nanoparticles which can then be used to covalently couple carbohydrates by way of the CH insertion reaction of photochemically activated PFPA (Scheme 1). Phosphate-functionalized PFPA photocoupling agents **1** and **2** were synthesized, where **1** contains ethylene oxide units which are polar and hydrophilic, whereas **2** has methylene units, which are nonpolar and hydrophobic. The ethylene oxide linkage has the additional property of being protein resistant; thus, it has been widely used to create biocompatible and antifouling surfaces (*44, 45*). Compounds **1** and **2** are prepared following the synthetic sequence shown in Scheme 2.

Spindle-type hematite α-Fe_2O_3 nanoparticles were synthesized by precipitating iron(III) perchlorate in the presence of urea and sodium dihydrogen phosphate, following a modified method by Ocaña (*41*). We found that, by adjusting experimental parameters such as the type of iron salt, the concentration, and the ionic strength of the solution, the size, morphology, and surface functionality of hematite nanoparticles can be controlled (*46*). Nanoparticles of ~250 nm and ~40 nm in equatorial diameters along the *x* and *y* axes, and ~40 nm in the polar diameter along the *z* axis, were synthesized and used in the present study. These particles were functionalized with **1** or **2** following a slightly modified literature method (*33*). In the experiment, nanoparticles were sonicated in the solution of **1** or **2** in $CHCl_3$ for 30 min followed by copious washing to remove the excess coupling

Scheme 2. Synthesis of Photocoupling Agents 1 and 2

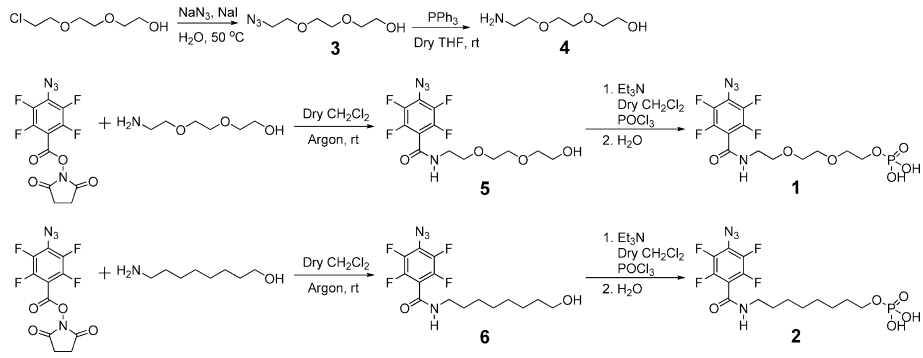

agent. The IR spectra of the resulting nanoparticles showed the azide ($-N_3$) antisymmetrical stretch at 2126 cm^{-1}, amide stretch at 1653 cm^{-1}, and P−O−C and P−O−Fe stretches from 1270 to 990 cm^{-1} (*47*), indicating that the nanoparticles have been successfully functionalized with the PFPA-phosphate coupling agent (Figure 1). Control studies were conducted with compounds **5** and **6** that are precursors of **1** and **2** and do not possess the phosphate group. The experiments were carried out following the same preparation procedure for **1**-NPs and **2**-NPs. The IR spectra of the resulting nanoparticles did not show the characeristic azide ($-N_3$) antisymmetrical stretch at 2126 cm^{-1} (Figure S3, Supporting Information), demonstrating that the phosphate group in **1** and **2** is responsible for the attachment of these coupling agents to the nanoparticles.

The successful surface functionalization of the nanoparticles was further supported by a solvent dispersion study. Nanoparticles functionalized with **1** or **2** (**1**-NPs, **2**-NPs) were mixed and sonicated in different solvents of water, ethanol, and acetonitrile. As shown in Figure 2, **1**-NPs dispersed well in water and ethanol but precipitated in acetonitrile. **2**-NPs, however, showed the opposite behavior; the particles precipitated in water and ethanol but dispersed well in acetonitrile. The ethylene oxide linkage in **1** is capable of forming hydrogen bonds with protic solvents of water and ethanol, thus improving the miscibility of the resulting nanoparticles in these media (*48, 49*). Acetonitrile, lacking the hydrogen bonding ability, is more compatible with the hydrophobic alkyl linkage in **2**. Therefore, depending on the nature of the ligands to be attached, the corresponding coupling agent can be selected, for example, **1** for aqueous-soluble molecules and **2** for organic solvent-soluble compounds. For carbohydrates that are highly polar and water soluble, **1** was used as the coupling agent, and **1**-NPs were used throughout the study.

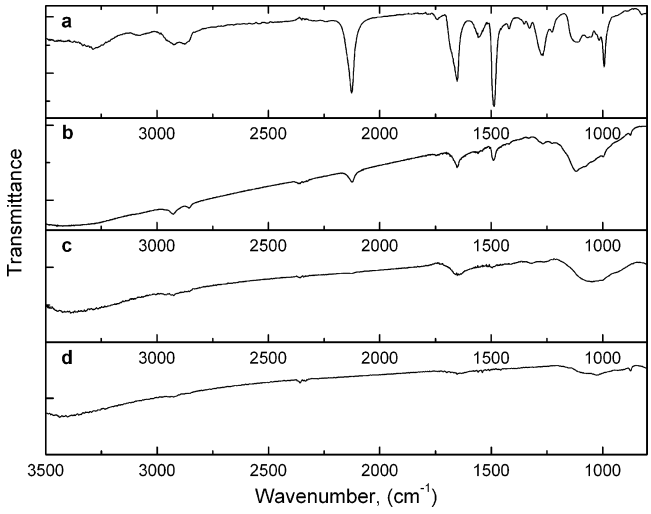

Figure 1. FTIR spectra of (a) PFPA-phosphate ligand **1**; (b) hematite nanoparticles functionalized with **1**; (c) nanoparticles coupled with D-mannose; (d) unfunctionalized hematite nanoparticles.

Subsequent coupling of carbohydrates to **1**-NPs were carried out using D-mannose. Monosaccharides are the smallest carbohydrate structures and the most challenging for this coupling chemistry. The probability of the CH insertion reaction increases as the size of the carbohydrate structure or the number of CH bonds increases. Additionally, monosaccharides are the lowest-affinity ligands, therefore lacking the multivalency effect that can occur in their oligosaccharide counterparts (*50*). Thus, if these monosaccharide ligands can be successfully coupled to NPs, and the resulting conjugated ligands retain their recognition abilities, the methodology developed can be readily applied to other large and more complicated carbohydrate structures. The coupling reaction was carried out by irradiating a mixture of **1**-NPs and the monosaccharide in water/ethanol for 30 min while stirring. The $-N_3$ absorption at 2126 cm^{-1} disappeared in the IR spectrum of the resulting nanoparticles (Figure 1c) indicating that the azide was activated. The surface property of the NPs changed after the monosaccharide coupling. While the as-prepared hematite NPs tend to agglomerate (Figure 3a), NPs coated with D-mannose were well-separated (Figure 3b). In addition, the D-mannose-coated NPs were readily dispersed in water to give a homogeneous dispersion.

The amount of carbohydrate ligands bound to the nanoparticles was determined by the thermogravimetric analysis (TGA). TGA measures the mass loss of the organic materials as they decompose upon heating. When TGA was conducted on **1**-NPs and mannose-**1**-NPs, the percentage mass changes relative to the weight of the hematite NPs were small and within the experimental error of the instrument. To overcome this problem, smaller iron oxide nanoparticles were prepared to increase the percentage of the organic mass relative to that of the nanoparticles. Spherical superparamagnetic Fe_3O_4 nanoparticles of ∼10 nm in diameter were synthesized by the coprecipatation method according to the literature procedure (*4, 42*). The particles were functionalized with **1**, and the subsequent D-mannose coupling was carried out following the same protocol described above for the hematite NPs. Figure 4 shows the weight loss of each sample as a function of heating temperature. The unfunctionalized NPs showed a decrease in mass up to ∼400 °C, probably due to the presence of volatile residuals trapped inside the nanoparticles. Compared to the unfunctionalized NPs, nanoparticles functionalized with **1** showed a 3.3% weight loss at 600 °C accounting for the mass of the coupling agent. After D-mannose was attached to the nanoparticles, weight loss of

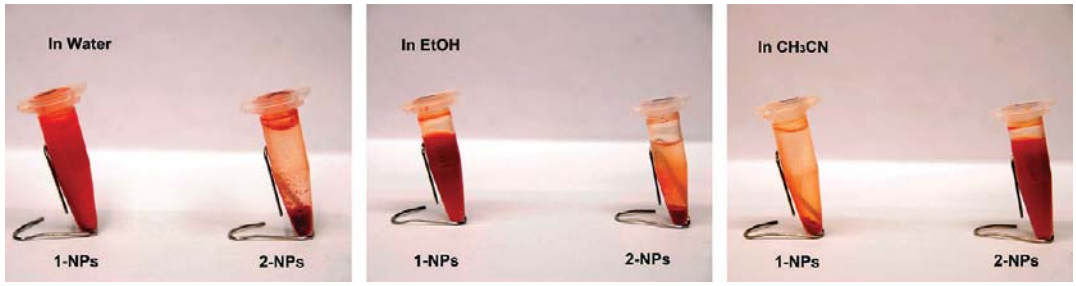

Figure 2. Functionalized nanoparticles **1**-NPs and **2**-NPs in water, ethanol, and acetonitrile (~3.3 mg/mL). Samples were sonicated for 30 min and allowed to settle for over 2 h.

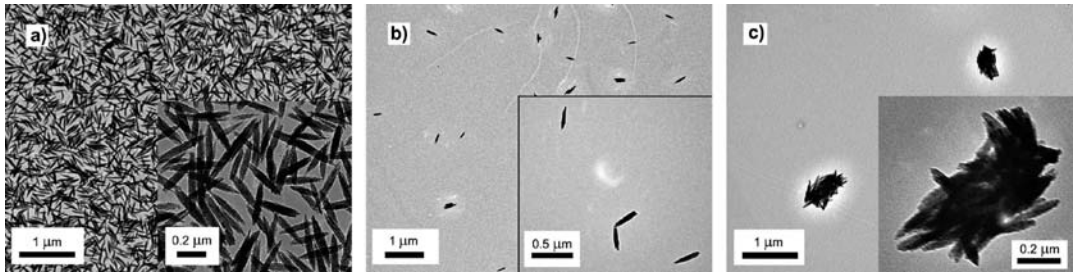

Figure 3. TEM images of (a) hematite nanoparticles, (b) mannose-**1**-NPs (500 μg/mL), and (c) subsequent treatment with *Con A*.

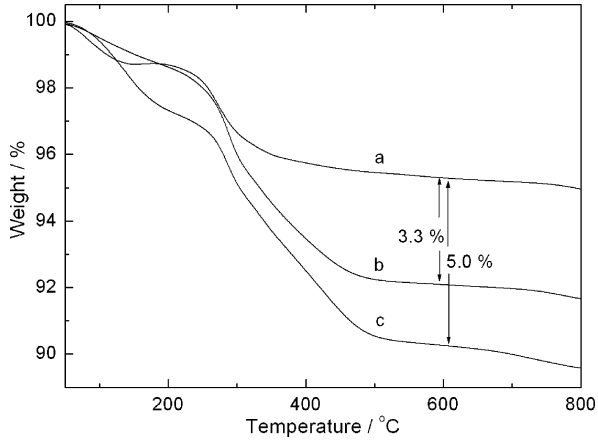

Figure 4. TGA curves of (a) Fe_3O_4 nanoparticles; (b) **1**-Fe_3O_4-NPs; (c) mannose-**1**-Fe_3O_4-NPs.

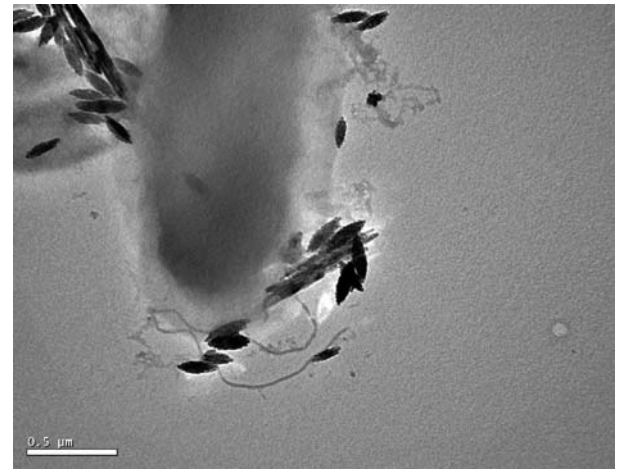

Figure 5. TEM images of *E. coli* ORN178 strain after treating with mannose-functionalized hematite nanoparticles.

5.0% at 600 °C was observed. This corresponds to the combined mass of D-mannose and the coupling agent **1**.

On the basis of these results, the number of organic molecules on each nanoparticle (N) can be calculated from eq 1

$$N = \frac{\frac{4}{3}\pi r^3 \rho w}{\mathrm{MW}} N_\mathrm{A} \qquad (1)$$

where w is the percentage of the weight loss (%), r is the radius of the Fe_3O_4 nanoparticles (averaged 5 nm by TEM), N_A is the Avogadro number, ρ is the density of Fe_3O_4 (5.1 g/cm^3 or 5.1 $\times$ 10^{-21} g/nm^3), and MW is the formula weight of the organic molecule after attaching to the nanoparticle (446 g/mol for **1** and 626 g/mol for mannose-**1** linked to nanoparticle surface). Therefore, weight losses of 3.3% and 5.0% correspond to 119 PFPA-phosphate ligands **1** and 128 mannose-**1** on one nanoparticle surface, respectively. This result means that there are roughly the same number of the coupling agent and the coupled D-mannose on the nanoparticles, indicating that the carbohydrate coupling reaction is fairly efficient.

The mannose-functionalized hematite NPs were subsequently evaluated to test if the conjugated D-mannose retains its recognition ability. *Con A*, a plant lectin that specifically binds mannopyranoside and glucopyranosides (*39, 50, 51*), was chosen for this study. Above pH 7, *Con A* exists as a tetramer with each face having two binding sites for the carbohydrate ligand. When mannose-**1**-NPs were treated with *Con A*, they assembled into bundled clusters (Figure 3c). Note that the mannose-**1**-NPs were well-dispersed before binding with *Con A* (Figures 3b). The aggregation can be explained by considering *Con A* as an equivalent of a tetrafunctional cross-linking agent, which upon interacting with D-mannose on NPs, brings together the nanoparticles forming a cross-linked network structure (*52*).

The recognition ability of D-mannose tethered to the hematite NPs was further evaluated in a bacteria binding study. Two *E. coli* strains, ORN178 and ORN208, were selected (*53*). ORN 178 has a mannose specific binding domain, i.e., the FimH lectin on type 1 pili, whereas ORN 208 is deficient of mannose-binding FimH protein (*53*−*57*). After the mannose-**1**-NPs were incubated with ORN 178, spindle nanoparticles were observed attaching themselves at the lateral ends and along the pili of the bacteria (Figure 5) (*53, 54, 58*). The strong binding between the nanoparticles

and the pili of ORN178 can be attributed to the multivalent interactions between the surface-confined mannose with the FimH lectin domain on type 1 pili. On the contrary, nanoparticles were absent on the *E. coli* ORN208 strain confirming the FimH-specific binding of the mannose ligands.

CONCLUSIONS

In summary, phosphate-containing PFPA coupling agents were synthesized and applied to functionalize iron oxide nanoparticles. Monosaccharides were successfully coupled to PFPA-functionalized nanoparticles by the photochemically induced CH insertion reaction of PFPA, which does not require chemical derivatization of the carbohydrate structures. The immobilized carbohydrates retained their recognition abilities, as demonstrated by the strong affinity with their corresponding carbohydrate-binding proteins and bacteria. The method developed can be readily applied to other carbohydrate structures including oligosaccharides, polysaccharides, and glycoconjugates. This general coupling chemistry, together with the magnetic properties of iron oxide nanoparticles, offer an attractive platform for rapid qualitative clinical diagnosis, decontamination of biological threats, and biomedical applications.

ACKNOWLEDGMENT

The authors thank the financial support from NIH (R01GM-080295-01 and R15GM066279-02), and ONAMI ARL Center. We gratefully acknowledge financial support from the Adolphe Merkle Foundation and the Swiss National Science Foundation. We thank Professor Paul E. Orndorff (North Carolina State University) for providing *E. coli* ORN178 and ORN208 strain, Professor Ken Stedman and Mr. Jim Laidler for discussions and assistance with *E. coli* experiment, Mr. Xin Wang for TEM images.

Supporting Information Available: ^{1}H NMR spectra of **1** and **2**, and FTIR of control experiments.

LITERATURE CITED

(1) Paulson, J. C., Blixt, O., and Collins, B. E. (2006) Sweet spots in functional glycomics. *Nat. Chem. Biol. 2*, 238–248.

(2) Stevens, J., Blixt, O., Paulson, J. C., and Wilson, I. A. (2006) Glycan microarray technologies: tools to survey host specificity of influenza viruses. *Nat. Rev. Microbiol. 4*, 857–864.

(3) Wang, H. F., Gu, L. R., Lin, Y., Lu, F. S., Meziani, M. J., Luo, P. G. J., Wang, W., Cao, L., and Sun, Y. P. (2006) Unique aggregation of anthrax (*Bacillus anthracis*) spores by sugar-coated single-walled carbon nanotubes. *J. Am. Chem. Soc. 128*, 13364–13365.

(4) El-Boubbou, K., Gruden, C., and Huang, X. (2007) Magnetic glyco-nanoparticles: A unique tool for rapid pathogen detection, decontamination, and strain differentiation. *J. Am. Chem. Soc. 129*, 13392–13393.

(5) Ngundi, M. M., Kulagina, N. V., Anderson, G. P., and Taitt, C. R. (2006) Nonantibody-based recognition: alternative molecules for detection of pathogens. *Exp. Rev. Proteomics 3*, 511–524.

(6) Laurent, N., Voglmeir, J., and Flitsch, S. L. (2008) Glycoarrays - tools for determining protein-carbohydrate interactions and glycoenzyme specificity. *Chem. Commun.* 4400–4412.

(7) Liang, P. H., Wang, S. K., and Wong, C. H. (2007) Quantitative analysis of carbohydrate-protein interactions using glycan microarrays: Determination of surface and solution dissociation constants. *J. Am. Chem. Soc. 129*, 11177–11184.

(8) Disney, M. D., and Seeberger, P. H. (2004) The use of carbohydrate microarrays to study carbohydrate-cell interactions and to detect pathogens. *Chem. Biol. 11*, 1701–1707.

(9) Park, S., Lee, M. R., Pyo, S. J., and Shin, I. (2004) Carbohydrate chips for studying high-throughput carbohydrate-protein interactions. *J. Am. Chem. Soc. 126*, 4812–4819.

(10) Brun, M. A., Disney, M. D., and Seeberger, P. H. (2006) Miniaturization of microwave-assisted carbohydrate functionalization to create oligosaccharide microarrays. *ChemBioChem 7*, 421–424.

(11) Michel, O., and Ravoo, B. J. (2008) Carbohydrate microarrays by microcontact "click" chemistry. *Langmuir 24*, 12116–12118.

(12) Bryan, M. C., Fazio, F., Lee, H. K., Huang, C. Y., Chang, A., Best, M. D., Calarese, D. A., Blixt, C., Paulson, J. C., Burton, D., Wilson, I. A., and Wong, C. H. (2004) Covalent display of oligosaccharide arrays in microtiter plates. *J. Am. Chem. Soc. 126*, 8640–8641.

(13) Lee, M., and Shin, I. (2005) Facile preparation of carbohydrate microarrays by site-specific, covalent immobilization of unmodified carbohydrates on hydrazide-coated glass slides. *Org. Lett. 7*, 4269–4272.

(14) Zhi, Z. L., Powell, A. K., and Turnbull, J. E. (2006) Fabrication of carbohydrate microarrays on gold surfaces: Direct attachment of nonderivatized oligosaccharides to hydrazide-modified self-assembled monolayers. *Anal. Chem. 78*, 4786–4793.

(15) Xia, B. Y., Kawar, Z. S., Ju, T. Z., Alvarez, R. A., Sachdev, G. P., and Cummings, R. D. (2005) Versatile fluorescent derivatization of glycans for glycomic analysis. *Nat. Methods 2*, 845–850.

(16) Seo, J. H., Adachi, K., Lee, B. K., Kang, D. G., Kim, Y. K., Kim, K. R., Lee, H. Y., Kawai, T., and Cha, H. J. (2007) Facile and rapid direct gold surface immobilization with controlled orientation for carbohydrates. *Bioconjugate Chem. 18*, 2197–2201.

(17) Ito, Y. (2006) Photoimmobilization for microarrays. *Biotechnol. Prog.* 924–932.

(18) Carroll, G. T., Wang, D. N., Turro, N. J., and Koberstein, J. T. (2008) Photons to illuminate the universe of sugar diversity through bioarrays. *Glycoconjugate J. 25*, 5–10.

(19) Carroll, G. T., Wang, D. N., Turro, N. J., and Koberstein, J. T. (2006) Photochemical micropatterning of carbohydrates on a surface. *Langmuir 22*, 2899–2905.

(20) Yan, M. (2007) Photochemically initiated single polymer immobilization. *Chem. Eur. J. 13*, 4138–4144.

(21) Pei, Y. X., Yu, H., Pei, Z. C., Theurer, M., Ammer, C., Andre, S., Gabius, H. J., Yan, M., and Ramstrom, O. (2007) Photoderivatized polymer thin films at quartz crystal microbalance surfaces: Sensors for carbohydrate-protein interactions. *Anal. Chem. 79*, 6897–6902.

(22) Pei, Z. C., Yu, H., Theurer, M., Walden, A., Nilsson, P., Yan, M., and Ramstrom, O. (2007) Photogenerated carbohydrate microarrays. *ChemBioChem 8*, 166–168.

(23) Liu, L., Engelhard, M. H., and Yan, M. (2006) Surface and interface control on photochemically initiated immobilization. *J. Am. Chem. Soc. 128*, 14067–14072.

(24) Liu, L., and Yan, M. (2006) A general approach to the covalent immobilization of single polymers. *Angew. Chem., Int. Ed. 45*, 6207–6210.

(25) Lu, A. H., Salabas, E. L., and Schuth, F. (2007) Magnetic nanoparticles: Synthesis, protection, functionalization, and application. *Angew. Chem., Int. Ed. 46*, 1222–1244.

(26) Laurent, S., Forge, D., Port, M., Roch, A., Robic, C., Elst, L. V., and Muller, R. N. (2008) Magnetic iron oxide nanoparticles: Synthesis, stabilization, vectorization, physicochemical characterizations, and biological applications. *Chem. Rev. 108*, 2064–2110.

(27) Gupta, A. K., and Gupta, M. (2005) Synthesis and surface engineering of iron oxide nanoparticles for biomedical applications. *Biomaterials 26*, 3995–4021.

(28) Neouze, M. A., and Schubert, U. (2008) Surface modification and functionalization of metal and metal oxide nanoparticles by organic ligands. *Monatsh. Chem. 139*, 183–195.
(29) Latham, A. H., and Williams, M. E. (2008) Controlling transport and chemical functionality of magnetic nanoparticles. *Acc. Chem. Res. 41*, 411–420.
(30) Veiseh, O., Sun, C., Gunn, J., Kohler, N., Gabikian, P., Lee, D., Bhattarai, N., Ellenbogen, R., Sze, R., Hallahan, A., Olson, J., and Zhang, M. Q. (2005) Optical and MRI multifunctional nanoprobe for targeting gliomas. *Nano Lett. 5*, 1003–1008.
(31) De Palma, R., Peeters, S., Van Bael, M. J., Van den Rul, H., Bonroy, K., Laureyn, W., Mullens, J., Borghs, G., and Maes, G. (2007) Silane ligand exchange to make hydrophobic superparamagnetic nanoparticles water-dispersible. *Chem. Mater. 19*, 1821–1831.
(32) Mutin, P. H., Guerrero, G., and Vioux, A. (2005) Hybrid materials from organophosphorus coupling molecules. *J. Mater. Chem. 15*, 3761–3768.
(33) White, M. A., Johnson, J. A., Koberstein, J. T., and Turro, N. J. (2006) Toward the syntheses of universal ligands for metal oxide surfaces: Controlling surface functionality through click chemistry. *J. Am. Chem. Soc. 128*, 11356–11357.
(34) Bin Na, H., Lee, I. S., Seo, H., Il Park, Y., Lee, J. H., Kim, S. W., and Hyeon, T. (2007) Versatile PEG-derivatized phosphine oxide ligands for water-dispersible metal oxide nanocrystals. *Chem. Commun.* 5167–5169.
(35) Matsuno, R., Yamamoto, K., Otsuka, H., and Takahara, A. (2004) Polystyrene- and poly(3-vinylpyridine)-grafted magnetite nanoparticles prepared through surface-initiated nitroxide-mediated radical polymerization. *Macromolecules 37*, 2203–2209.
(36) Georgelin, T., Moreau, B., Bar, N., Villemin, D., Cabuil, V., and Horner, O. (2008) Functionalization of gamma-Fe_2O_3 nanoparticles through the grafting of an organophosphorous ligand. *Sens. Actuators, B 134*, 451–454.
(37) Yee, C., Kataby, G., Ulman, A., Prozorov, T., White, H., King, A., Rafailovich, M., Sokolov, J., and Gedanken, A. (1999) Self-assembled monolayers of alkanesulfonic and -phosphonic acids on amorphous iron oxide nanoparticles. *Langmuir 15*, 7111–7115.
(38) Griep-Raming, N., Karger, M., and Menzel, H. (2004) Using benzophenone-functionalized phosphonic acid to attach thin polymer films to titanium surfaces. *Langmuir 20*, 11811–11814.
(39) Lis, H., and Sharon, N. (1998) Lectins: Carbohydrate-specific proteins that mediate cellular recognition. *Chem. Rev. 98*, 637–674.
(40) Keana, J. F. W., and Cai, S. X. (1990) New reagents for photoaffinity-labeling - synthesis and photolysis of functionalized perfluorophenyl azides. *J. Org. Chem. 55*, 3640–3647.
(41) Ocana, M., Morales, M. P., and Serna, C. J. (1999) Homogeneous precipitation of uniform alpha-Fe_2O_3 particles from iron salts solutions in the presence of urea. *J. Colloid Interface Sci. 212*, 317–323.
(42) Cheng, F. Y., Su, C. H., Yang, Y. S., Yeh, C. S., Tsai, C. Y., Wu, C. L., Wu, M. T., and Shieh, D. B. (2005) Characterization of aqueous dispersions of Fe_3O_4 nanoparticles and their biomedical applications. *Biomaterials 26*, 729–738.
(43) Sezonov, G., Joseleau-Petit, D., and D'Ari, R. (2007) *Escherichia coli* physiology in Luria-Bertani broth. *J. Bacteriol. 189*, 8746–8749.
(44) Harris, J. M. (1992) in *Poly(Ethylene Glycol) Chemistry* Plenum, New York.
(45) Harder, P., Grunze, M., Dahint, R., Whitesides, G. M., and Laibinis, P. E. (1998) Molecular conformation in oligo(ethylene glycol)-terminated self-assembled monolayers on gold and silver surfaces determines their ability to resist protein adsorption. *J. Phys. Chem. B 102*, 426–436.
(46) Dietsch, H., Malik, V., Reufer, M., Dagallier, C., Shalkevich, A., Saric, M., Gibaud, T., Cardinaux, F., Scheffold, F., Stradner, A., and Schurtenberger, P. (2008) Soft nanotechnology - from colloid physics to nanostructured functional materials. *Chimia 62*, 805–814.
(47) Daou, T. J., Begin-Colin, S., Greneche, J. M., Thomas, F., Derory, A., Bernhardt, P., Legare, P., and Pourroy, G. (2007) Phosphate adsorption properties of magnetite-based nanoparticles. *Chem. Mater. 19*, 4494–4505.
(48) Zolk, M., Eisert, F., Pipper, J., Herrwerth, S., Eck, W., Buck, M., and Grunze, M. (2000) Solvation of oligo(ethylene glycol)-terminated self-assembled monolayers studied by vibrational sum frequency spectroscopy. *Langmuir 16*, 5849–5852.
(49) Wang, R. L. C., Kreuzer, H. J., and Grunze, M. (2000) The interaction of oligo(ethylene oxide) with water: a quantum mechanical study. *Phys. Chem. Chem. Phys. 2*, 3613–3622.
(50) Dam, T. K., and Brewer, C. F. (2002) Thermodynamic studies of lectin-carbohydrate interactions by isothermal titration calorimetry. *Chem. Rev. 102*, 387–429.
(51) Bouckaert, J., Loris, R., Poortmans, F., and Wyns, L. (1995) Crystallographic structure of metal-free concanavalin A at 2.5 angstrom resolution. *Proteins: Struct., Funct., Bioinf. 23*, 510–524.
(52) Gupta, D., Bhattacharyya, L., Fant, J., Macaluso, F., Sabesan, S., and Brewer, C. F. (1994) Observation of unique cross-linked lattices between multiantennary carbohydrates and soybean lectin - presence of pseudo-2-fold axes of symmetry in complex type carbohydrates. *Biochemistry 33*, 7495–7504.
(53) Lin, C. C., Yeh, Y. C., Yang, C. Y., Chen, C. L., Chen, G. F., Chen, C. C., and Wu, Y. C. (2002) Selective binding of mannose-encapsulated gold nanoparticles to type 1 pili in *Escherichia coli*. *J. Am. Chem. Soc. 124*, 3508–3509.
(54) Krogfelt, K. A., Bergmans, H., and Klemm, P. (1990) Direct evidence that the fimh protein is the mannose-specific adhesin of *Escherichia coli* type-1 fimbriae. *Infect. Immun. 58*, 1995–1998.
(55) Choudhury, D., Thompson, A., Stojanoff, V., Langermann, S., Pinkner, J., Hultgren, S. J., and Knight, S. D. (1999) X-ray structure of the FimC-FimH chaperone-adhesin complex from uropathogenic *Escherichia coli*. *Science 285*, 1061–1066.
(56) Harris, S. L., Spears, P. A., Havell, E. A., Hamrick, T. S., Horton, J. R., and Orndorff, P. E. (2001) Characterization of *Escherichia coli* type 1 pilus mutants with altered binding specificities. *J. Bacteriol. 183*, 4099–4102.
(57) Tchesnokova, V., Aprikian, P., Yakovenko, O., Larock, C., Kidd, B., Vogel, V., Thomas, W., and Sokurenko, E. (2008) Integrin-like allosteric properties of the catch bond-forming FimH adhesin of *Escherichia coli*. *J. Biol. Chem. 283*, 7823–7833.
(58) Ryu, J. H., Lee, E., Lim, Y. B., and Lee, M. (2007) Carbohydrate-coated supramolecular structures: Transformation of nanofibers into spherical micelles triggered by guest encapsulation. *J. Am. Chem. Soc. 129*, 4808–4814.